JOURNAL OF AIRCRAFT
Vol. 41, No. 5, September–October 2004

Preliminary Design of a Structural Wing Box Under a Twist Constraint Part I

Rakesh K. Kapania* and Sangeon Chun†
Virginia Polytechnic Institute and State University, Blacksburg, Virginia 24061-0203

We present a simple beam-type formulation to determine the structural weight of a wing to carry aerodynamic loads in a transonic flowfield. The formulation employs nondimensional or scaled parameters and thus can be easily integrated with aerodynamic codes that often provide aerodynamic loads using scaled variables, for example, TOPS, developed at NASA Ames Research Center. The formulation first uses a simple double-plate model to determine the material required to withstand the bending. This double-plate model is then transformed into a hexagonal box model using empirical data to represent the torsional stiffness. To prevent large twist of the wing, a constraint that restricts the maximum rate of twist in a wing segment to 0.1 radian per wing semispan is used. The angle of twist near the tip is found to be significantly impacted by two parameters: the sweep of the elastic axis and the chord-wise location of a structural wing box. Optimization approaches are used to find these two parameters so that the overall aerodynamic torque acting on the elastic axis is minimized. The results from the method of steepest-descent and the conjugate-gradient method are compared with those of genetic algorithms. A good agreement is obtained.

Nomenclature

A = reference area of the half of a wing
$\bar{A}$ = nondimensionlized reference area
b = aerodynamic semispan
$\bar{b}$ = nondimensionalized aerodynamic semispan
$\bar{b}_i$ = nondimensionalized y coordinate value at the ith node of a wing
b_{st} = structural semispan
C_m = pitching-moment coefficient about the aerodynamic reference axis
C_R = root chord of a wing
C_T = tip chord of a wing
$\bar{C}_T$ = nondimensionalized tip chord
C_Z = nondimensionalized aerodynamic force coefficient in the z direction
C_Z^R = force coefficient obtained for the root segment
C_Z^{total} = total force coefficient
d_i = thickness of the ith segment of a wing
$\bar{d}_i$ = nondimensionalized thickness of the ith segment of a wing
e_i = nondimensionalized relative coordinate value from an elastic axis to an aerodynamic reference axis
$\bar{M}_i$ = nondimensionalized bending moment acting at the ith node
N_l = load factor
N_s = number of the nodes for a semiwing
q_0 = measure of force per unit length at the root
q_∞ = freestream dynamic pressure
S_f = safety factor
$\bar{S}_i$ = nondimensionalized shear force acting at the ith node
s = constant chordwise position of a line along the span
$\bar{T}_i$ = nondimensionalized total torque acting at the ith node
t_i = thickness of each panel of the ith segment of a wing
$W_{\text{T.O.}}$ = takeoff weight
$\bar{w}_i$ = nondimensionalized bending deflection at the ith node
$\bar{x}_{\text{rear}}$ = nondimensionalized relative coordinate value from $x = \frac{3}{4}$ to the rear spar position at the root
x_{ref} = x-coordinate value of an aerodynamic reference axis
$\bar{x}_{\text{ref}}$ = nondimensionalized x coordinate value of an aerodynamic reference axis
$\bar{x}_0$ = nondimensionalized x coordinate value of the elastic axis at the root
α_i = adjusting factor for the ith wing segment
γ = weight density of the plate material
$\Delta\bar{b}_i$ = nondimensionalized span of the ith segment of a wing
$\Delta\bar{S}_i$ = nondimensionalized shear force acting on the ith segment of a wing semispan
ΔT_i = torque acting on the ith wing segment
θ_i = angle of twist at the ith node
Λ_{LE} = sweep angle of the leading edge of the wing
Λ_s = sweep angle of the line defined by s
σ_{all} = allowable bending stress of the plate material

Introduction

In recent years there has been a considerable interest in developing revolutionary aircraft concepts.[1] In the design of these aircrafts, it is important that an accurate structural model be available to determine the structural weight of a wing and various interactive responses between different disciplines be included as early as possible in the design cycle. One of the most important interactions that must be taken into account early in the design process is the aeroelastic coupling. Often during the preliminary design, the emphasis is only on determining the structural weight to carry the critical wing bending. This can be accomplished very easily using a double-plate beam model. The double-plate model is, however, inadequate to represent the torsional stiffness of a wing because this model is an open-section model. A number of approaches to obtain dimensions of an equivalent dimension of a closed-section model from which the torsional stiffness can be calculated using the double-plate model information were described by Sulaeman et al.[2]

An alternative approach, which was based on a closed-section model obtained using empirical data, was made available to us by Lockheed Martin as part of a joint collaborative work on a strut-braced wing. This hexagonal box model, used successfully to perform design of a strut-braced wing by Gern et al.,[3,4] is used in the present study.

When used for designing transonic wings, however, it was observed that this hexagonal box model did not give adequate torsional

Presented as Paper 2003-2004 at the AIAA/ASME/ASCE/AHS 44th Structures, Structural Dynamics, and Materials Conference, Norfolk, VA; received 4 February 2003; revision received 2 July 2003; accepted for publication 10 July 2003. Copyright © 2003 by the American Institute of Aeronautics and Astronautics, Inc. All rights reserved. Copies of this paper may be made for personal or internal use, on condition that the copier pay the $10.00 per-copy fee to the Copyright Clearance Center, Inc., 222 Rosewood Drive, Danvers, MA 01923; include the code 0021-8669/04 $10.00 in correspondence with the CCC.

*Professor, Department of Aerospace and Ocean Engineering. Associate Fellow AIAA.
†Graduate Research Assistant, Department of Aerospace and Ocean Engineering.

stiffness near the wing tip. For some cases we observed significant twisting of the wing near the tip, and these large angles of twist caused a very detrimental effect during the aerodynamic calculations. To prevent this large twist problem, we implemented a maximum twist rate constraint that prevented the wing from having excessive torsional flexibility. This was accomplished by restricting the rate of twist of a given wing segment to 0.1 radian per wing semispan. This means that under no circumstance the aeroelastic twist rate of any segment can be bigger than 0.1 radian/unit length for a given wing. A value of the twist rate constraint less than this value can have a significant effect on the wing weight. Similarly, a value of the twist rate constraint larger than 0.1 can make the wing very flexible under torsion.

The angles of twist of the wing near the tip region, as can be expected, are significantly influenced by two parameters: 1) the sweep angle of a structural wing box and 2) the chordwise location of the rear spar of the structural wing box along the root chord of the wing. We selected the values of these parameters such that a measure of overall torque around the elastic axis of the wing is minimized. To obtain this minimum value, we employed three optimization approaches: 1) genetic algorithms (GAs),[5] 2) the method of steepest descent,[6,7] and 3) the conjugate-gradient method.[7] The reason GAs were used first is to obtain the global minimum in the search space of unknown surface characteristics because GAs are well known for their robustness.[5] Then gradient-based methods of steepest descent and conjugate gradient were applied to obtain the minimum values, and these values were compared with the values from GAs. Because the values of both the parameters obtained from all of the three methods were in good agreement, a gradient-based method of conjugate gradient was finally selected based on the computational efficiency for the optimization process in implementing the maximum twist rate constraint. To ensure that the values of the two variables, as given by the gradient-based methods, stay within physically meaningful ranges, a special treatment for side constraints on their respective values was devised.

The simple beam-type model, using a preselected set of values of the sweep angle and the relative location along the root chord of a wing for the elastic axis, was successfully employed in designing wings under aeroelastic interactions. This was accomplished using genetic algorithms to determine designs that maximize both the lift-to-drag ratio and the inverse of the structural weight. Details of that study are available elsewhere.[8]

Wing Bending Weight

The structural wing model used in this study is a simple beam-type model that is capable of resisting aerodynamic loads without failing caused by excessive bending and/or excessive twist in transonic flights. Details of the structural model and a way to implement a constraint to prevent excessive twist are given in the following sections.

Shear Force and Bending Moment Distribution

The aerodynamic wing shape, provided to the TOPS code, is given in terms of C_R, and the wing semispan is divided into N_s stations (see Fig. 1). The aerodynamic loads from the full potential code TOPS are given to these divided segments in terms of C_Z and C_m (refer to Appendix and Fig. 2). These coefficients are normalized with respect to the nondimensionalized wing semispan area. Therefore the actual physical force acting on a segment can be obtained by multiplying C_Z with q_∞, C_R^2 and $\bar{A}$; $\bar{A} = A/C_R^2$. TOPS give the force coefficient for each aerodynamic wing segment divided by $\bar{A}$.

The shear force and the bending moment for the beam are nondimensionalized with respect to $q_0 b_{\text{st}}$, and $q_0 b_{\text{st}}^2$, respectively, that is, $\bar{S} = S/q_0 b_{\text{st}}$ and $\bar{M} = M/q_0 b_{\text{st}}^2$. Here b_{st} is given as

$$b_{\text{st}} = b/\cos\Lambda_s = (\bar{b}/\cos\Lambda_s)C_R \tag{1}$$

When modeled as a beam, the wing is assumed to be a cantilever beam along the same direction as indicated by this structural semispan line b_{st}. Λ_s is given as

$$\tan\Lambda_s = \tan\Lambda_{\text{LE}} - s[(1 - \bar{C}_T)/\bar{b}] \tag{2}$$

where $\bar{C}_T$ is nondimensionalized with respect to C_R, that is, $\bar{C}_T = C_T/C_R$. Generally, the value of s lies between 0.5 and 0.75 and plays a significant role in determining the torque and hence the resulting twist deformation of the tip of the wing box.

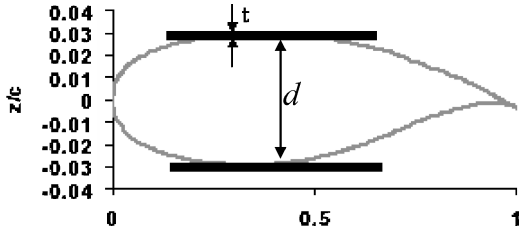

a) Double plate

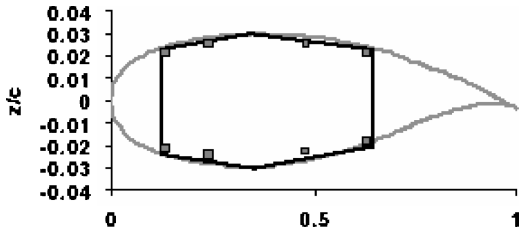

b) Hexagonal box

Fig. 2 Wing-section models used for structural analysis in the preliminary design of a wing.

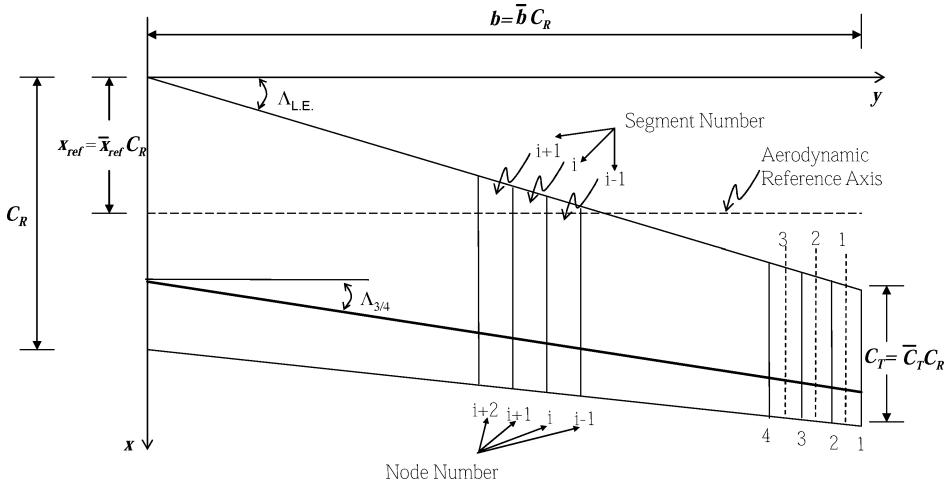

Fig. 1 Wing planform and its discretization for calculating the structural response.

The quantity q_0, used for nondimensionalizing the shear force and bending moment diagram, is given by

$$q_0 = \frac{W_{\text{T.O.}} C_Z^R}{2 b_{\text{st}} C_Z^{\text{total}}} \tag{3}$$

$W_{\text{T.O.}}$ is given as

$$W_{\text{T.O.}} = 2 q_\infty \bar{A} C_R^2 C_Z^{\text{total}} \tag{4}$$

Substituting Eq. (4) into Eq. (3), q_0 is given as

$$q_0 = q_\infty \bar{A} C_R C_Z^R \cos \Lambda_s \big/ \bar{b} \tag{5}$$

$\Delta \bar{S}_i$ for a unit load factor is given as

$$\Delta \bar{S}_i = \frac{\Delta S_i}{q_0 b_{\text{st}}} = \frac{q_\infty \bar{A} C_R^2 C_{\text{Zi}}}{q_0 b_{\text{st}}} = \frac{C_{\text{Zi}}}{C_Z^R}, \qquad 1 \le i \le N_s - 1 \tag{6}$$

$\bar{S}_i$ at the ith node can be obtained by adding all of the shear forces on the segments between that node and the tip.

$$\bar{S}_i = \bar{S}_{i-1} + \Delta \bar{S}_{i-1} = \sum_{j=1}^{i-1} \Delta \bar{S}_j \tag{7}$$

The node number for this analysis starts from the tip, and thus the shear force at the wing tip S_1 is zero (see Fig. 1). $\bar{M}_{i+1}$ at the $i+1$th node can be written as

$$\bar{M}_{i+1} = \bar{M}_i - (\bar{S}_i + 0.5 \Delta \bar{S}_i)(\Delta \bar{b}_i / \bar{b}) \tag{8}$$

Wing Bending Weight Estimation

To obtain the weight of the material required to carry the bending loads, we treated the wing as a beam with a cross section consisting of two panels at a distance d, that is, a double-plate model shown in Fig. 2. The t_i, required to carry the bending stress, can be obtained using the flexural formula

$$t_i = \frac{S_f N_l M_i}{C_b^i d_i \sigma_{\text{all}}} \tag{9}$$

In Eq. (9) N_l is taken to be 2.5, S_f is taken to be 1.5, d_i is taken to be the maximum thickness of the airfoil for preliminary analysis purposes. C_b^i is the structural chord (width) of the ith wing segment, and it is assumed to be 50% of the aerodynamic chord in the present study as the front spar is generally placed at 15% of the aerodynamic chord and the rear spar is generally placed at 65% of the aerodynamic chord. Finally σ_{all} is nondimensionalized as

$$\bar{\sigma}_{\text{all}} = \frac{\sigma_{\text{all}} b_{\text{st}}}{q_0} = \frac{\sigma_{\text{all}} \bar{b}^2}{q_\infty \bar{A} C_Z^R \cos^2 \Lambda_s} \tag{10}$$

The total wing weight W can be obtained as

$$W = \sum_{i=1}^{N_s - 1} \Delta W_i = \sum_{i=1}^{N_s - 1} 2 \gamma C_b^i t_i \alpha_i \frac{\Delta b_i}{\cos \Lambda_s} \tag{11}$$

where α_i is used to increase the panel thickness in each segment to satisfy nonstress constraints. Because the value of t_i obtained from Eq. (9) must often be increased to satisfy other constraints, namely, divergence, flutter, or perhaps, as in this study, on the angle of twist. For example, the thickness obtained from the bending analysis might be even lower than the minimum gauge requirement driven by manufacturing considerations. To account for all of these constraints, the value of t_i, given by Eq. (9), was multiplied by α_i.

The weight of the bending material in terms of nondimensional quantities can be written as

$$W = 2 \gamma b_{\text{st}}^3 S_f N_l \sum_{i=1}^{N_s - 1} \alpha_i \frac{\bar{M}_i}{\bar{\sigma}_{\text{all}}} \frac{\Delta \bar{b}_i}{\bar{d}_i \cos \Lambda_s} \tag{12}$$

Wing Deflections

To obtain the deflection caused by bending and the angle of twist, the hexagonal wing model obtained from Lockheed Martin and used in our earlier studies on the strut-braced wing is employed. For that model (see Fig. 2b) it is assumed that the shear center lies near the middle of the wing box. The bending and the twist equations are integrated along the elastic axis of the beam, which is assumed to pass through a pre-selected chordwise location x_0 along the root and make an angle of Λ_s with the y axis (see Fig. 3). Both the location of x_0 and the angle Λ_s play a major role in determining the overall torque to which the wing will be subjected.

Bending Deflection and Slope

The governing equation for the bending deflection along the elastic axis y_l (see Fig. 3) is written as

$$EI \frac{\mathrm{d}^2 w}{\mathrm{d} y_l^2} = M(y_l) \tag{13}$$

where EI is the bending stiffness of a beam.

Consider the following nondimensionalization:

$$w = b_{\text{st}} \bar{w} \tag{14}$$

$$y_l = b_{\text{st}} \bar{y} \tag{15}$$

$$t_i = b_{\text{st}} \bar{t}_i \tag{16}$$

$$C_b^i = b_{\text{st}} \bar{C}_b^i \tag{17}$$

$$d_i = b_{\text{st}} \bar{d}_i \tag{18}$$

$$E = \bar{E} q_0 / b_{\text{st}} \tag{19}$$

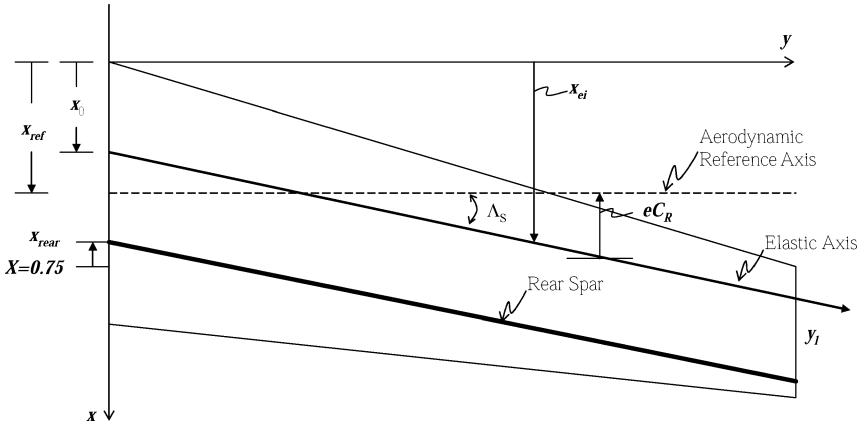

Fig. 3 Definition of an elastic axis, an aerodynamic reference axis, and rear spar.

Using the preceding scaling and recalling the fact that for the double-plate model the moment of inertia for the ith segment of the beam is given as $I_i = C_{\text{bi}} t_i d_i^2/2$, Eq. (13) becomes

$$\frac{\mathrm{d}^2\bar{w}}{\mathrm{d}\bar{y}_l^2} = 2\frac{N_l \bar{M}_i}{\bar{E}\bar{C}_b^i \alpha_i \bar{t}_i \bar{d}_i^2} \tag{20}$$

In Eq. (20) N_l is the load factor and $\bar{M}_i$ is the nondimensionalized bending moment for the ith wing segment for a unit load factor. The bending moment is assumed to be constant for each segment. This is obviously an approximation, but it will yield quite accurate results as the number of beam segments is increased. Substituting, in Eq. (20), the value of t_i as obtained for a load factor of 2.5 and a safety factor of 1.5, from Eq. (9), we get

$$\frac{\mathrm{d}^2\bar{w}}{\mathrm{d}\bar{y}_l^2} = \frac{2N_l}{3.75}\frac{\bar{\sigma}_{\text{all}}}{\bar{E}\alpha_i \bar{d}_i} \tag{21}$$

where the ratio $\bar{E}_i/\bar{\sigma}_{\text{all}}$ is taken to be 185 for the present analysis.

For calculating the slope caused by bending and the bending deflection, we assume the beam to be piecewise uniform. The $\bar{w}_i$ and the scaled slope $(\mathrm{d}\bar{w}/\mathrm{d}\bar{y})_i$ at the ith node can be obtained by integrating Eq. (21) with respect to $\bar{y}$ from the root shown as

$$\left(\frac{\mathrm{d}\bar{w}}{\mathrm{d}\bar{y}}\right)_i = \left(\frac{\mathrm{d}\bar{w}}{\mathrm{d}\bar{y}}\right)_{i+1} + \frac{2N_l}{3.75}\frac{\bar{\sigma}_{\text{all}}}{\bar{E}\alpha_i \bar{d}_i}\left(\frac{\Delta\bar{b}_i}{\bar{b}}\right) \tag{22}$$

$$\bar{w}_i = \bar{w}_{i+1} + \left(\frac{\mathrm{d}\bar{w}}{\mathrm{d}\bar{y}}\right)_{i+1}\left(\frac{\Delta\bar{b}_i}{\bar{b}}\right) + \frac{N_l}{3.75}\frac{\bar{\sigma}_{\text{all}}}{\bar{E}\alpha_i \bar{d}_i}\left(\frac{\Delta\bar{b}_i}{\bar{b}}\right)^2 \tag{23}$$

Recall that nodes are numbered from tip ($i = 1$) to root ($i = N_s$), and the nondimensionalized deflection and the scaled slope are determined along the elastic axis of the wing box. At the root ($i = N_s$) both the deflection and the slope vanish.

Angle of Twist

The angle of twist can be obtained in the same way. The wing box is divided into a number of uniform segments. The torsional stiffness for the beam was obtained from the hexagonal box model. The torsion acting on the wing can be obtained at each of the nodes of the wing box in terms of the shear force and the pitching moment. The aerodynamic code TOPS provides C'_m about an aerodynamic reference axis, which lies at $x = x_{\text{ref}}$ (see Fig. 3). Recall that the coordinate system for TOPS passes through the intersection of the leading edge of the wing with wing root and that the geometry of the wing is expressed in terms of the root chord. Assuming that the reference aerodynamic axis lies in front of the elastic axis with $e_i C_R$, ΔT_i can be expressed as

$$\Delta T_i = q_0 b_{\text{st}}^2 \Delta\bar{T}_i$$

$$\Delta\bar{T}_i = \left[\left(C_{Z\text{i}}/C_Z^R\right)e_i + C_{mi}/C_Z^R\right]\left(\cos^2\Lambda_s/\bar{b}\right) \tag{24}$$

where we have made use of Eqs. (5) and (6). In Eq. (24) the torque is assumed to be positive if it twists the leading edge in the upward direction (nose up). $e_i C_R$ is shown as (see Fig. 3)

$$e_i C_R = (\bar{x}_0 + \bar{b}_i \tan\Lambda_s - \bar{x}_{\text{ref}})C_R \tag{25}$$

The reference aerodynamic axis in calculating the pitching moments was assumed to be passing through the root midchord, leading to $x_{\text{ref}} = 0.5$. Therefore e_i can be expressed as

$$e_i = (-\bar{x}_{\text{rear}} + \bar{b}_i \tan\Lambda_s) \tag{26}$$

The nondimensionalized total torque $\bar{T}_{i+1}$ ($T = \bar{T} q_0 b_{\text{st}}^2$), acting at the $i+1$th node, can be expressed as

$$\bar{T}_{i+1} = \left[\left(C_{Zi}/C_Z^R\right)(\bar{b}_i \tan\Lambda_s - \bar{x}_{\text{rear}}) + C_{mi}/C_Z^R\right]\left(\cos^2\Lambda_s/\bar{b}\right) \tag{27}$$

The angles of twist can be obtained by solving the twist equation about the elastic axis. The elastic axis is also the locus of the center of twist. The governing equation, for the ith segment, can be written as

$$(GJ)_i \frac{\mathrm{d}\theta}{\mathrm{d}y_l} = T_i \tag{28}$$

where $(GJ)_i$ is the effective torsional stiffness of the ith hexagonal box. As was done for the case of bending deflection, the relevant quantities such as shear modulus G, torsional stiffness GJ, and the coordinate y_l can be scaled as

$$y_l = b_{\text{st}}\bar{y} \tag{29}$$

$$G = \frac{\bar{G}q_0}{b_{\text{st}}} \tag{30}$$

$$GJ = q_0 b_{\text{st}}^3 \overline{GJ}, \qquad \overline{GJ} = q_0 b_{\text{st}}^3 \frac{[2\bar{A}_{\text{en}}]^2}{\oint d\bar{s}/\bar{G}\bar{t}} \tag{31}$$

$$\frac{\mathrm{d}}{\mathrm{d}y_l} = \frac{\mathrm{d}}{b_{\text{st}}\,\mathrm{d}\bar{y}} \tag{32}$$

In Eq. (31) A_{en} is the area enclosed by the box. Because all of the dimensions and the thicknesses of the box beam are given in terms of b_{st}, the wing structural semispan A_{en} is given by $b_{\text{st}}^2 \bar{A}_{\text{en}}$. The scaling given by Eqs. (29–32) will reduce the governing equation, Eq. (28), for the ith segment in a nondimensional form, as follows:

$$(\overline{GJ})_i \frac{\mathrm{d}\theta}{\mathrm{d}\bar{y}} = \bar{T}_i \tag{33}$$

The torque on the segment i is taken to be uniform with a value given by the average of the torques on its two endpoints i and $i+1$. The value of $\overline{GJ}$ is obtained from an empirical hexagonal box model.

The angle of twist θ_i at the ith node can be obtained by integrating Eq. (33) with respect to $\bar{y}$ from the root shown as

$$\theta_i = \theta_{i+1} + (\bar{T}_i/\overline{GJ})(\Delta\bar{b}_i/\bar{b}) \tag{34}$$

Using the $\overline{GJ}$ values, as obtained from the hexagonal box model, very large values of $\mathrm{d}\theta/\mathrm{d}\bar{y}$ were found near the wing tip. From Eq. (27) it is obvious that both $\bar{x}_{\text{rear}}$ and s from Eq. (2) defining Λ_s play an important role in determining the value of the overall torque acting on the wing. This is especially true as one approaches the tip of a wing having a high aspect ratio. An ill-conceived selection of the parameters $\bar{x}_{\text{rear}}$ and s leads to a relatively large value of torque near the wing tip. Towards the tip of the wing, the value of the bending stiffness is extremely small. Because the torsional stiffness, as given by the empirical model used in this study, is related to the value of the bending stiffness, the torsional stiffness will also be very small. This will result in a large value of the angle of twist.

To overcome this problem, two steps were taken to reduce the angle of twist.

1) Using optimization methods, the values of $\bar{x}_{\text{rear}}$ and s were chosen to minimize the overall torque around the elastic axis of the wing Φ, defined as

$$\Phi = \sum_{i=1}^{N_s} \bar{T}_i^2 \tag{35}$$

As shown in Eqs. (2) and (27), $\bar{T}$ was a function of $\bar{x}_{\text{rear}}$ and s, and so Φ is also a function of $\bar{x}_{\text{rear}}$ and s. Figure 4 shows contours of the function Φ for two arbitrary aerodynamic loading cases.

2) A maximum twist rate constraint was implemented such that the value of $\Delta\theta/\Delta\bar{y} = \bar{T}_i/\overline{GP}$ in a given segment does not go beyond a certain value (say between 0.1 to 0.2 radian per span length). If for any segment the value of $\Delta\theta/\Delta\bar{y}_i$ does go beyond the constraint

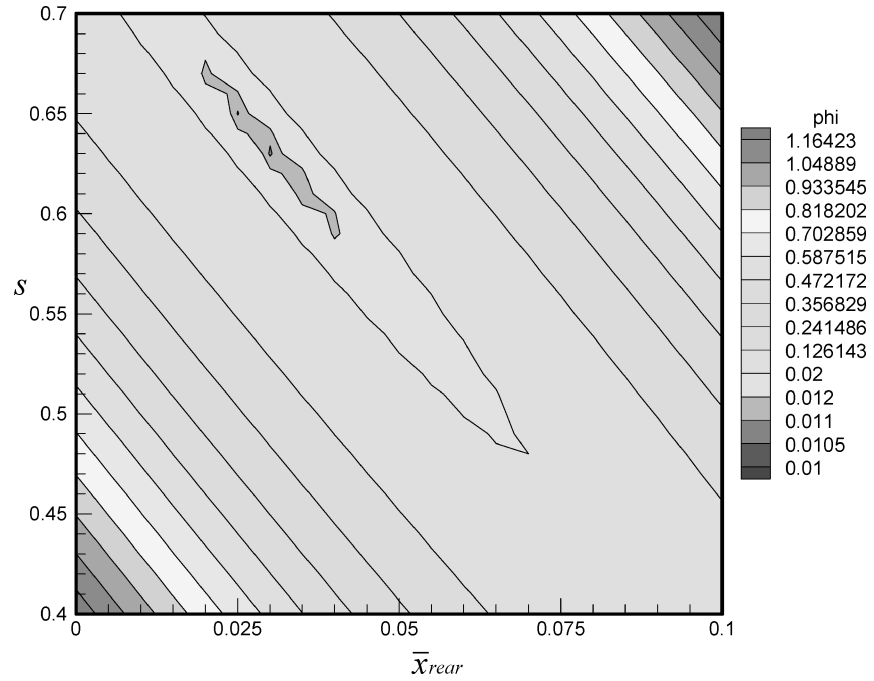

a) Without active constraint

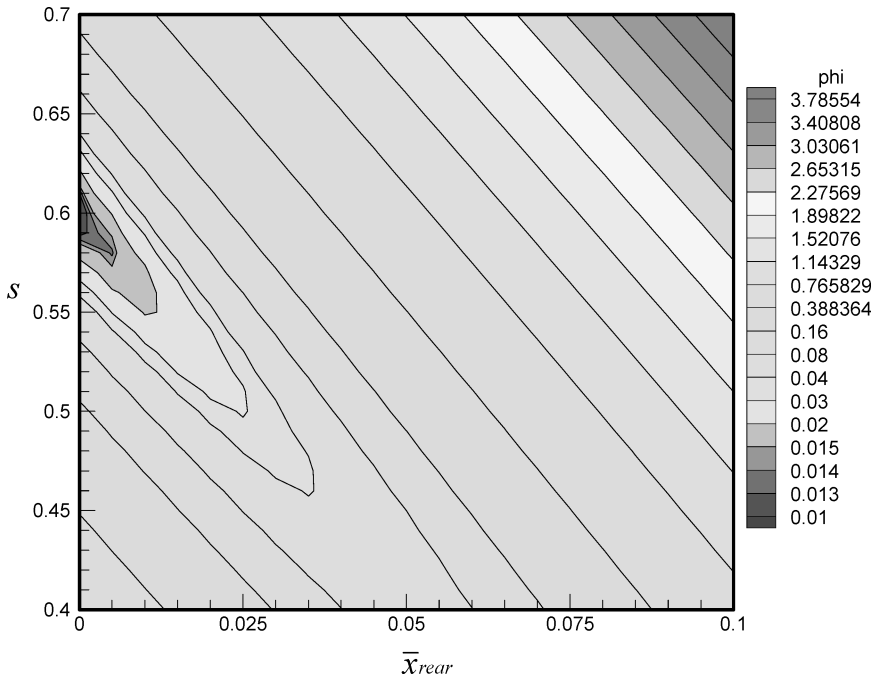

b) With active constraint

Fig. 4 Contours of a function Φ for two arbitrary aerodynamic loading cases.

value, the value of $\overline{GJ}$ for that segment was increased to reduce the value of $\Delta\theta/\Delta\bar{y}_i$ to the specified constraint for this ratio. Naturally, this will result in an increased weight.

Taking the first step of minimizing the overall torque can reduce the number of segments for which the value of torsional stiffness has to be increased. For example, Fig. 4a shows the contour lines of different values of Φ in the $\bar{x}_{\text{rear}} - s$ plane for an example loading. One of the local minima for Φ can be observed near $s = 0.63$ (i.e., the elastic axis is along the direction that corresponds to the 63% chord) and $\bar{x}_{\text{rear}} = 0.03$. The minimum value was obtained at $s = 0.63$ and $\bar{x}_{\text{rear}} = 0.03$. This implies that the wing box must be placed at the same angle as that of the wing sweep corresponding to the 63% chord line and the inboard of the rear spar must be located at 72% of the root chord.

The geometry input to the aerodynamic code TOPS requires that along the aerodynamic reference axis, $\bar{\bar{w}}$ the wing deflection, nondimensionalized with respect to the root chord, and $\bar{\theta}$ the angle of twist about the aerodynamic reference axis be provided. These can be obtained as

$$\bar{\bar{w}}_i = \frac{w_a}{C_R} = \frac{\bar{b}\bar{w}_i}{\cos\Lambda_s} + e_i\bar{\theta}_i \tag{36}$$

$$\bar{\theta}_i = \theta_i \cos\Lambda_s - \left(\frac{\mathrm{d}\bar{w}}{\mathrm{d}\bar{y}}\right)_i \sin\Lambda_s \tag{37}$$

Here w_a is the transverse deflection at the aerodynamic reference axis, and e_i is given by Eq. (26).

Optimization

As explained in the preceding section on angle of twist, the twist angles near the tip of a wing can be significantly influenced by two parameters: 1) the sweep angle of a structural wing box and 2) the chordwise location of the rear spar of the structural wing box along the root chord of the wing. In this work we employed three optimization approaches: 1) genetic algorithms, 2) the method of steepest descent, and 3) the conjugate-gradient method. All three optimization methods were programmed in FORTRAN. Usually GAs are used for discrete variables, but here variables are continuous, and we selected a GA using real-valued chromosomes.[9] The reason GA was used in this work was to obtain the global minimum in the search space of unknown surface characteristics because GAs are well known for their robustness. Then gradient-based methods of steepest descent and conjugate gradient were applied to obtain the minimum values, and these values were compared with the values from GAs. To ensure that the values of the two variables, as given by the gradient-based methods, stay within physically meaningful ranges, the special treatment for side constraints on their respective values was devised. In case of GAs, a simple penalty function method[5] was used to keep the variables within the ranges of side constraints.

Constraint Treatment

For the gradient-based methods of steepest descent and conjugate gradient, treating active constraints is not simple, as compared to GAs, using a penalty function method. Here, a rather simple method is devised and used to deal with such cases. When the minimum point is out of the target range ($0.4 \le s \le 0.7$ and $0.0 \le \bar{x}_{\text{rear}} \le 0.1$), that is, side constraints are active, this point is shifted within the target range using the method explained in this section.

The background for this specially devised method comes from the characteristics of the search space in this work. As seen in Fig. 4a, the stationary point is located in a long, narrow valley, and the values of the vicinity of the minimum within the valley do not show significant differences from the minimum itself. Therefore, we can approximate the minimum value of the objective function with the value in the vicinity of that minimum value when the minimum point is out of the target range.

Based on the tendency of the valley shape, the vicinity point is found as follows (see Fig. 5):

Step 0: Use the steepest descent or the conjugate gradient to get the minimum point $s, \bar{x}_{\text{rear}}$) of a function Φ without side constraints. If this point is out of the target range ($0.4 \le s \le 0.7$ and $0.0 \le \bar{x}_{\text{rear}} \le 0.1$), that is, $\star$ in the Fig. 5, then do the following:

Step 1: Employ one-dimensional search for obtaining a minimum point of a function Φ (s) along the line of $\bar{x}_{\text{rear}} = 0.0$, termed s_1.

Step 2: Employ one-dimensional search for obtaining a minimum point of a function Φ (s) along the line of $\bar{x}_{\text{rear}} = 0.1$, termed s_2.

Step 3: Obtain an average value of s_1 and s_2, termed s_3. If s_3 is out of the target range ($0.45 \le s \le 0.65$), where the target range of s was reduced to keep the point from being on the side constraint lines, that is, $s = 0.4$ or 0.7, then step 4 will be performed before the step 5. Or if s_3 is within the target range ($0.45 \le s \le 0.65$), then step 5 will be performed without step 4.

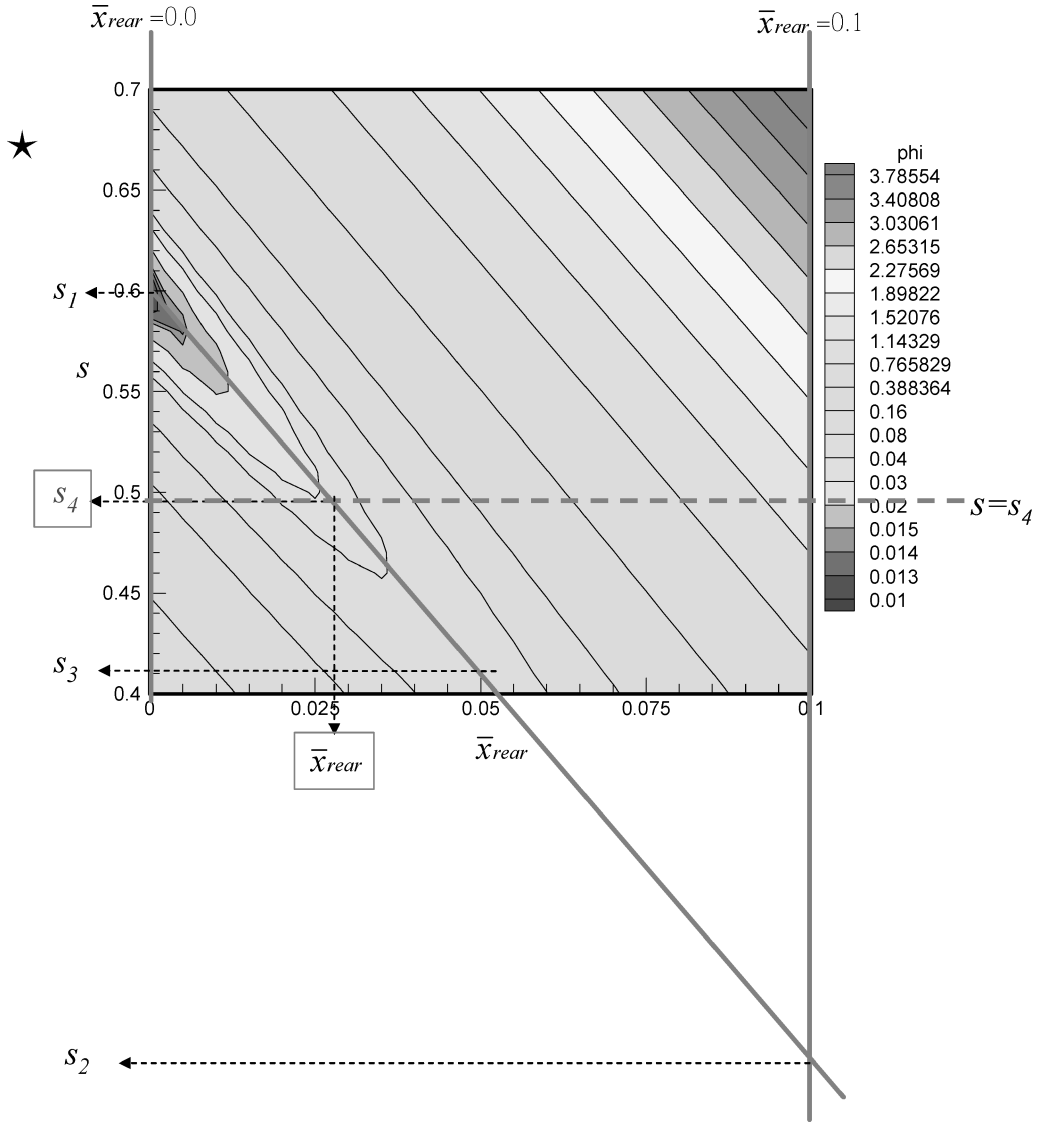

Fig. 5 Algorithm for the side-constraint treatment for two design variables $\bar{x}_{\text{rear}}$ and s.

Step 4: Move the s_3 value to s within the target range from 0.4 to 0.7, shown as 4 in Fig. 5, based on the following conditions:

If $s_3 > 0.7$ and $s_1 > 0.7$, then $s_3 = (0.7 + s_2)/2$.
Else if $s_3 > 0.7$ and $s_2 > 0.7$, then $s_3 = (0.7 + s_1)/2$.
Else if $s_3 < 0.4$ and $s_2 < 0.4$, then $s_3 = (0.4 + s_1)/2$.
Else if $s_3 < 0.4$ and $s_1 < 0.4$, then $s_3 = (0.4 + s_2)/2$.
Else if $s_3 > 0.65$ and $s_1 > 0.7$, then $s_3 = (0.7 + s_2)/2$.
Else if $s_3 > 0.65$ and $s_2 > 0.7$, then $s_3 = (0.7 + s_1)/2$.
Else if $s_3 < 0.45$ and $s_1 < 0.4$, then $s_3 = (0.4 + s_2)/2$.
Else if $s_3 < 0.45$ and $s_2 < 0.4$, then $s_3 = (0.4 + s_1)/2$.

Step 5: Employ one-dimensional search for obtaining a minimum point of a function $\Phi(\bar{x}_{\text{rear}})$ along the line of s, termed $\bar{x}_{\text{rear}}$.

Results

A genetic algorithm using real-valued chromosomes was applied to two aerodynamic load conditions shown in Fig. 4 to obtain the optimum design values: one is the case without active constraints and the other is with active constraints. In both cases GA parameters are chosen as follows: population = 20, crossover probability = 0.9, generation gap = 0.95, and mutation probability = 0.5 (Ref. 5).

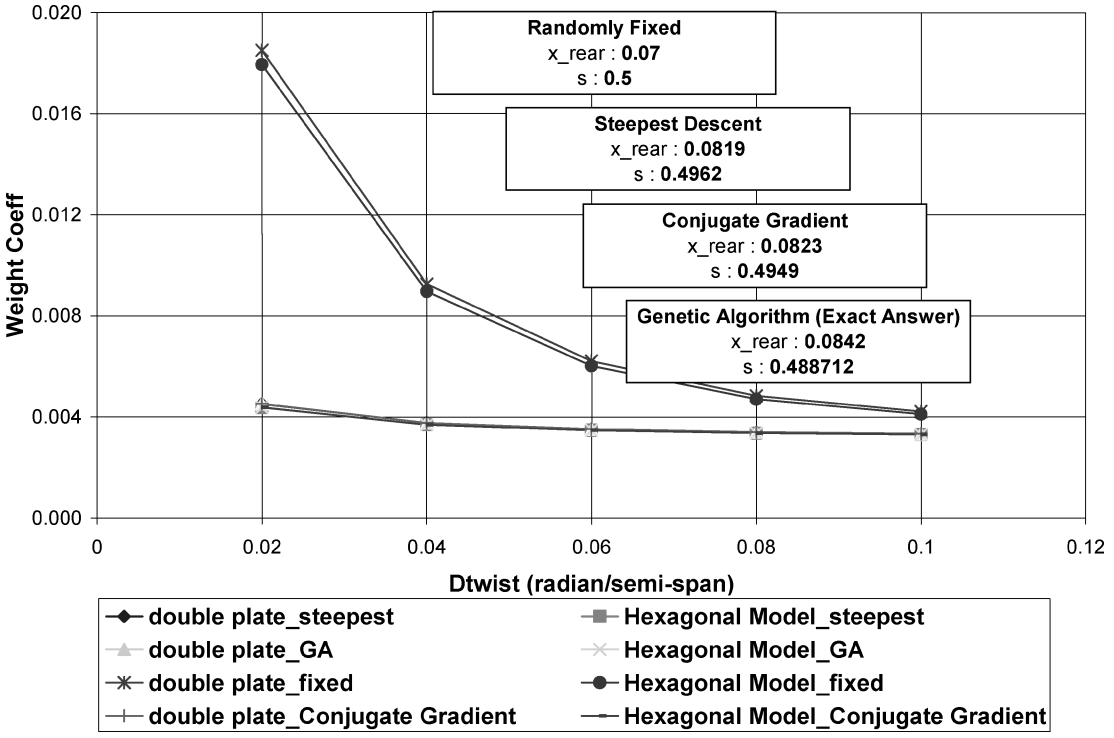

Fig. 6a Variation of the structural weight as a function of the twist rate constraint without active side constraints.

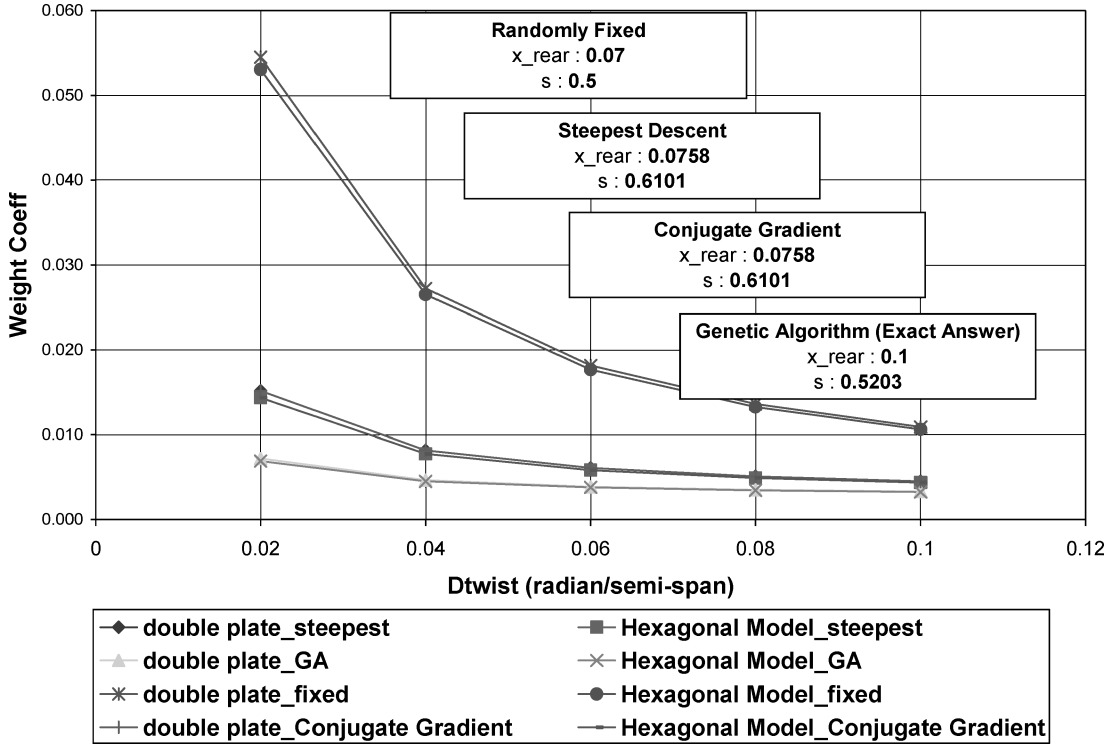

Fig. 6b Variation of the structural weight as a function of the twist rate constraint with active side constraints.

This GA optimization reached the minimum value of the overall torque Φ about 40–60 generations.

Next, the gradient-based methods of steepest descent and conjugate gradient were tested for the case without active constraints, and the values of both the parameters obtained from these methods were found to be in good agreement with the ones from GAs (see Fig. 6a). Therefore, based on the computational efficiency gradient-based methods were determined to be used for the optimization process in implementing the maximum twist rate constraint.

Then, a total of 14 aerodynamic load cases were tested with GAs and gradient-based methods of steepest descent and conjugate gradient with the special treatment for side constraints. A genetic algorithm using real-value encoded chromosomes was used to see the difference between the minimum value from GA and vicinity value from the subroutine that incorporates side constraints.

From Fig. 6 we can figure out two important things. First, Fig. 6 shows that there is no significant difference among three optimization methods. When the minimum point is within the target range in Fig. 6a, the results are almost identical. But when the minimum point is out of the target range in Fig. 6b, there is a little difference between GAs and gradient-based methods.

The reason is that although GAs penalty function method finds the minimum value along the active constraint boundary the present vicinity-point approach in gradient-based methods locates the minimum value inside the target ranges. Second, the structural weight of a wing increased under the twist constraints as expected. Comparing

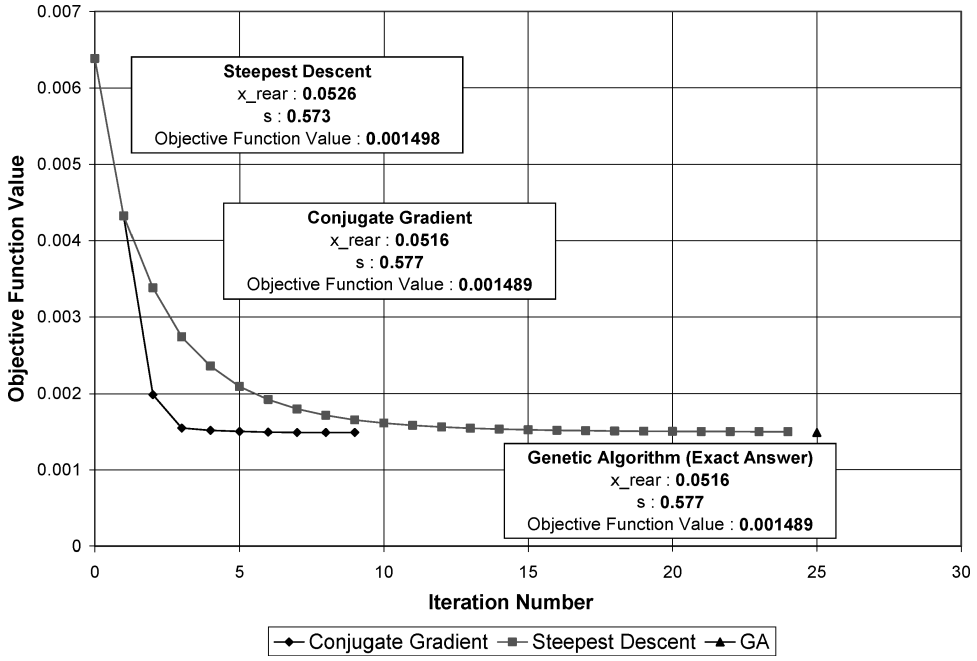

Fig. 7a Convergence tendencies of steepest descent and conjugate gradient without active side constraints (a maximum twist rate constraint = 0.1 radian per wing semispan).

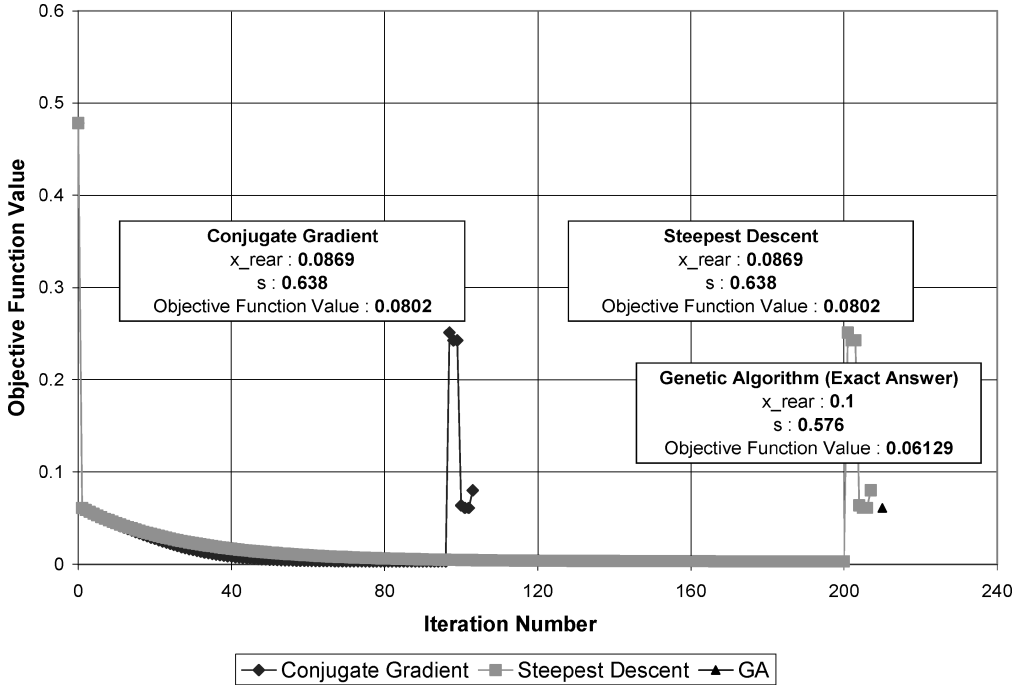

Fig. 7b Convergence tendencies of steepest descent and conjugate gradient with active side constraints (a maximum twist rate constraint = 0.1 radian per wing semispan).

weight coefficients from two different sets of $\bar{x}_{\text{rear}}$ and s in which one set of values is arbitrarily selected and the other set is obtained from optimization, we can see that the optimization of $\bar{x}_{\text{rear}}$ and s can reduce the increase in the weight by implementing the maximum twist rate constraint. Therefore, as the maximum twist rate constraint becomes dominant this optimization procedure becomes more and more important in saving the structural weight of a wing.

Figure 7a shows the most general convergence tendency in gradient-based optimization methods, namely, the conjugate-gradient method converges faster than the steepest-descent method. From all results it was observed that more than 70% of all of the cases show this tendency. Also, 23% cases show the case in which the number of iterations required in the conjugate-gradient method is more than the one required in the steepest-descent method, but the tendency is almost same with the results shown in Fig. 7a if the stopping criterion is raised slightly. Only 7% of all of the cases studied show the different tendency in which steepest-descent method converges faster than conjugate-gradient method. Figure 7b shows the convergence tendency in which the subroutine for the side-constraint treatment was used. Only two or three iterations were required for one-dimensional minimization used in the subroutine.

From the aforementioned results, we can conclude that the conjugate-gradient method, along with the subroutine to incorporate the special treatment for side constraints of $0.4 \le s \le 0.7$ and $0.0 \le \bar{x}_{\text{rear}} \le 0.1$, can be used to obtain the optimum values of $\bar{x}_{\text{rear}}$ and s for reducing the overall torque along the elastic axis of a wing.

Conclusions

The structural wing model of a double plate and a hexagonal box were used to show the effect of a maximum twist rate constraint on the calculation of the structural weight of a wing. In this research the maximum rate of twist in a wing segment such as 0.1 radian per wing semispan was used for the twist constraint. From the results this maximum twist rate constraint approach was found to be both effective and simple to implement in the aircraft design using the structural wing model.

The angle of twist near the tip, subjected to be compared with the twist constraints, was found to be significantly impacted by two parameters in the present study: 1) the sweep angle of the structural wing box and 2) the chordwise location of the rear spar of a structural wing box along the root chord of the wing. Therefore to reduce the weight increase caused by the twist constraints the optimized values of $\bar{x}_{\text{rear}}$ and s were obtained using three optimization methods (genetic algorithms, the method of steepest descent, and the conjugate-gradient method) before the twist constraints were implemented. For the treatment of side constraints of $\bar{x}_{\text{rear}}$ and s, which are needed to restrict the obtained values of the two parameters in a physically meaningful range, a rather simple subroutine was developed for the gradient-based methods. Through the numerical tests the conjugate-gradient method with the subroutine for the side-constraint treatment was found to successfully and efficiently obtain the optimized values of $\bar{x}_{\text{rear}}$ and s.

The structural wing model of a double plate and a hexagonal box incorporating the maximum twist rate constraint has been successfully integrated with the aerodynamic code TOPS to perform the preliminary aeroelastic design of a transonic wing using genetic algorithms.

Appendix: Aerodynamic Force Coefficients

$$\Delta x_{i,j} = \frac{1}{2}(x_{i+1,j} - x_{i,j} + x_{i+1,j+1} - x_{i,j+1}) \tag{A1}$$

$$\Delta y_{i,j} = \frac{1}{2}(y_{i+1,j} - y_{i,j} + y_{i+1,j+1} - y_{i,j+1}) \tag{A2}$$

$$\Delta z_{i,j} = \frac{1}{2}(z_{i+1,j} - z_{i,j} + z_{i+1,j+1} - z_{i,j+1}) \tag{A3}$$

$$C_P = \frac{p - p_\infty}{q_\infty} \tag{A4}$$

$$C_{\text{Pavg}_{i,j}} = \frac{1}{2}(C_{P_{i+1,j}} + C_{P_{i,j}}) \tag{A5}$$

$$\Delta C_{x_{i,j}} = C_{\text{Pavg}_{i,j}} \Delta y_{i,j} \Delta z_{i,j} \tag{A6}$$

$$\Delta C_{z_{i,j}} = -C_{\text{Pavg}_{i,j}} \Delta x_{i,j} \Delta y_{i,j} \tag{A7}$$

$$\Delta C_{m_{i,j}} = z_{\text{DIST}} \Delta C_{x_{i,j}} - x_{\text{DIST}} \Delta C_{z_{i,j}} \tag{A8}$$

$$C_{x_{i,j}} = \sum_i \sum_j \Delta C_{x_{i,j}} \tag{A9}$$

$$C_{z_{i,j}} = \sum_i \sum_j \Delta C_{z_{i,j}} \tag{A10}$$

$$C_{m_{i,j}} = \sum_i \sum_j \Delta C_{m_{i,j}} \tag{A11}$$

$$\bar{A} = \frac{A}{C_R^2} \tag{A12}$$

$$C_x = \frac{C_x}{\bar{A}} \tag{A13}$$

$$C_z = \frac{C_z}{\bar{A}} \tag{A14}$$

$$C_m = \frac{C_m}{\bar{A}} \tag{A15}$$

Refered to Fig. A1 for subscripts i, j, and DIST.

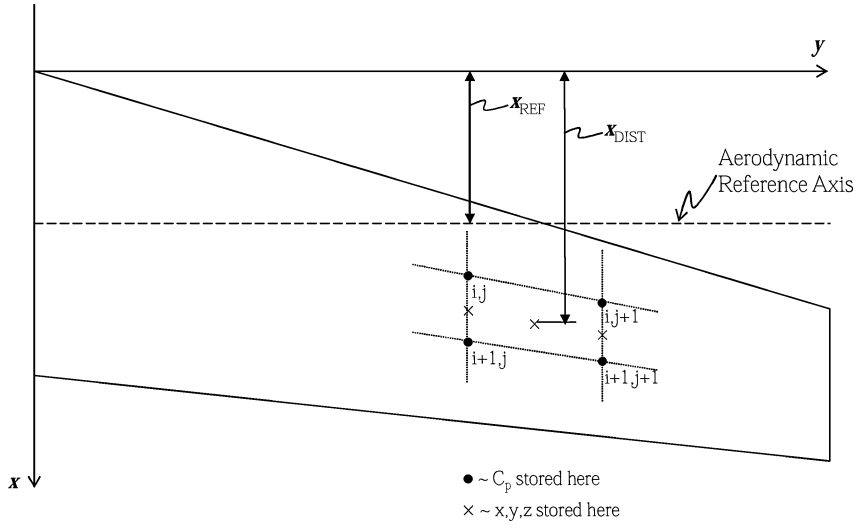

Fig. A1 Location and direction of elastic axis.

Acknowledgments

Portions of this work were performed under a consortium agreement NCC–2–5433 with NASA Ames Research Center. Technical discussions with Terry Holst of NASA Ames Research Center and Frank Gern of the Center for Intelligent Material Systems and Structures, Virginia Polytechnic Institute and State University are gratefully acknowledged.

References

[1]Blair, M., Moorhouse, D., and Weisshaar, T. A., "System Design Innovation Using Multidisciplinary Optimization and Simulation," AIAA Paper 2000-4705, Sept. 2000.

[2]Sulaeman, E., Kapania, R. K., and Haftka, R. T., "Parametric Studies on Aeroelastic Analysis of Strut Braced Wing," AIAA Paper 2002-1487, April 2002.

[3]Gern, F. H., Sulaeman, E., Naghshineh-Pour, A., Kapania, R. K., and Haftka, R. T., "Structural Wing Sizing for Multidisciplinary Design Optimization of a Strut-Braced Wing," *Journal of Aircraft*, Vol. 38, No. 1, 2001, pp. 154–163.

[4]Gern, F. H., Ko, A., Sulaeman, E., Gundlach, J. F., Kapania, R. K., and Haftka, R. T., "Multidisciplinary Design Optimization of a Transonic Commercial Transport with Strut-Braced Wing," *Journal of Aircraft*, Vol. 38, No. 6, 2001, pp. 1006–1014.

[5]Goldberg, D., *Genetic Algorithms in Search Optimization and Machine Learning*, Addison Wesley Longman, Reading, MA, 1989, pp. 1–25, 85, 86, 111.

[6]Burden, R. L., and Faires, J. D., *Numerical Analysis*, 7th ed., Brooks/Cole Publishing Co., Pacific Grove, CA, 2001, pp. 628–635.

[7]Vanderplaats, G. N., *Numerical Optimization Techniques for Engineering Design*, 3rd ed., Vanderplaats Research and Development, Inc., Colorado Springs, CO, 1999, pp. 103–108.

[8]Kapania, R. K., and Holst, T. L., "Aeroelastic Wing Optimization Using Genetic Algorithms," NASA Report, July 2002.

[9]Muhlenbein, H., and Schlierkamp-Voosen, D., "Predictive Models for the Breeder Genetic Algorithm: I. Continuous Parameter Optimization," *Evolutionary Computation*, Vol. 1, No. 1, 1993, pp. 25–49.

AIRCRAFT SYSTEMS:
Mechanical, Electrical, and Avionics Subsystems Integration
Ian Moir & Allan Seabridge

This text is designed to provide the reader with an introductory overview of the key system areas of commercial and military aircraft. It offers detailed illustration and a comprehensive explanation of the concepts and principles of system design, including the evolution of system design and the functionality of the contemporary design. It also identifies emerging technological breakthroughs that may have a profound effect upon the standard for avionics technology usage and associated systems integration.

The book serves as an introduction to the field of aerospace engineering for students, and provides a platform for practitioners wishing to update or extend their knowledge in light of technological advancements.

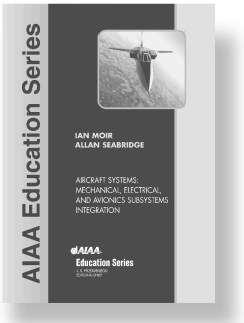

Copublished with Professional Engineering Publishing, publishers to the Institution of Mechanical Engineers.

Outside of the U.S., Call 44 1284 763 277 or Fax 44 1284 704 006

AIAA Education Series
2001, 350 pp, Hardcover • ISBN 1-56347-506-5
List Price: $99.95 • AIAA Member Price: $69.95
Source: 945

AIAA
American Institute of Aeronautics and Astronautics
Publications Customer Service, 9 Jay Gould Ct., P.O. Box 753, Waldorf, MD 20604
Fax 301/843-0159 Phone 800/682-2422 E-mail aiaa@tasco1.com
8 am–5 pm Eastern Standard Time
Order 24 hours a day at www.aiaa.org

CA and VA residents add applicable sales tax. For shipping and handling add $4.75 for 1–4 books (call for rates for higher quantities). All individual orders—including U.S., Canadian, and foreign—must be prepaid by personal or company check, traveler's check, international money order, or credit card (VISA, MasterCard, American Express, or Diners Club). All checks must be made payable to AIAA in U.S. dollars, drawn on a U.S. bank. Orders from libraries, corporations, government agencies, and university and college bookstores must be accompanied by an authorized purchase order. All other bookstore orders must be prepaid. Please allow 4 weeks for delivery. Prices are subject to change without notice. Returns in sellable condition will be accepted within 30 days. Sorry, we cannot accept returns of case studies, conference proceedings, sale items, or software (unless defective). Non-U.S. residents are responsible for payment of any taxes required by their government.

00-0349